# Fatigue Fracture of Reaction Injection Molded (RIM) Nylon Composites

D. C. MARTIN,* G. E. NOVAK, and M. G. WYZGOSKI, *Polymers Department, General Motors Research Laboratories, Warren, Michigan 48090-9055*

## Synopsis

This study was undertaken to determine how milled glass fibers affect the fatigue resistance of reaction injection molded (RIM) nylon 6. Specifically the effects of glass content, fiber length, orientation, and surface treatment were investigated. The fatigue crack growth rates for unfilled and glass-filled samples were observed to follow the well-known Paris equation in terms of dependence on cyclic stress intensity factor. For the unfilled nylon a line shaped zone was observed in advance of the crack tip. Fractography results suggest that the zone was the projection of the actual crack tip profile through the thickness of the sample rather than a distinct plastic or deformation zone. The fatigue fracture surface exhibited a patchy type structure with features 50–150 $\mu$m in size, suggesting a void coalescence type of mechanism as has been reported for injection molded nylons. A diffuse damage zone, several millimeters in size, was observed at the crack tip for the glass-filled RIM nylon 6. The zone was observed to pulsate with the applied oscillating load. The growth of the damage zone volume with increasing crack length (and thus increasing stress intensity factor range) followed the Paris law, as did the crack growth rate data. The damage mechanism is attributed to void formation and microcracking at the fiber–matrix interface. The results of this study show that, for milled glass-reinforced RIM nylon 6, the crack growth rates were much more rapid than observed for injection-molded nylon 6 containing chopped glass fibers. This difference is attributed to the greatly reduced glass fiber lengths for the milled glasses.

## INTRODUCTION

Reaction injection molding (RIM) represents an alternative processing method for the production of large plastic parts. Though it is employed primarily in the manufacture of polyurethane components, it is possible to use the RIM process to manufacture nylon 6 components via the anionic polymerization of caprolactam. It was therefore of interest to define the influence of dynamic loading on RIM nylon 6 and to compare the results with the commonly employed injection-molded nylons. Much has been written on the fatigue fracture behavior of nylon plastics due to the use of these materials in engineering applications.[1-4] Similarly the influence of glass fiber reinforcement on fatigue resistance has been investigated.[5] However, the conventional chopped glass fibers could not be used in a RIM process and consequently milled glass fibers having a shorter average length have been developed for this purpose.[6] Thus the influence of these newer milled glasses on the fatigue properties of RIM nylon were also of interest. This paper describes the fatigue

*Present address: University of Massachusetts, Amherst, MA.

Journal of Applied Polymer Science, Vol. 37, 3029–3056 (1989)
 CCC 0021-8995/89/103029-28$04.00

fracture behavior of both the unfilled and reinforced RIM nylon 6 in terms of the observed mechanical response and deformation mechanisms.

## EXPERIMENTAL

### Sample Preparation

RIM nylon 6 homopolymer was prepared by the anionic polymerization of caprolactam at 163°C. Sodium hydride was used as the initiator with toluene diisocyanate as a cocatalyst or activator. Table I lists the formulation which was prepared in two parts, preheated to the desired temperature, and mixed together just prior to hand pouring into a plaque mold.

Several types of milled glass fibers were added to the nylon in order to investigate size and surface treatment effects. A description of the fibers is given in Table II. All glasses were dried at 80°C in a vacuum oven overnight before use. The glass fiber lengths are considered maximum lengths, that is, all material will pass through a sieve of the stated size. The actual distribution of fiber lengths is not known but the milled glasses are reported to contain a significant fraction of rather small fiber fragments.[6] Test plaques, 203 × 203 × 3.2 mm, were prepared in aluminum sheet molds which were preheated to 163°C. After pouring, the molds were returned to the oven for 5 min to allow the polymerization reaction to proceed to completion. In some cases small bubbles would develop during pouring, causing porosity on the surface of the finished plaque, particularly near the edges. Though the exact cause of the bubbles was not determined, it was noted that more viscous mixtures showed less porosity. No samples which exhibited visible porosity were used for fatigue studies. The porosity did provide an unexpected benefit by indicating the general flow pattern in the mold as shown in Figure 1. Since the molten caprolactam was poured in at the top center, the pattern in Figure 1 suggests that the material flowed down the center of the vertically held mold with

TABLE I
RIM Nylon 6 Formulation

| Ingredients | Part A (parts) | Part B (parts) |
|---|---|---|
| Caprolactam | 100 | 100 |
| Sodium hydride | 0.8 | — |
| Toluene diisocyanate | — | 2 |
| Glass fibers | — | 35 or 100 |

TABLE II
Milled Glasses Added to RIM Nylon

| Source | Designation | Description |
|---|---|---|
| Henry and Frick Inc. | 3004 | 1/4 in., untreated |
| Henry and Frick Inc. | 3016 | 1/16 in., untreated |
| Henry and Frick Inc. | 3032 | 1/32 in., untreated |
| Owens-Corning Fiberglas Corp. | 737AA | 1/32 in., silane-treated |

subsequent flow up the sides. Though the orientation of glass fibers may differ somewhat from the porosity pattern shown here, it is clear that the overall orientation may vary considerably from point to point in a given plaque. For the glass-reinforced plaques the exact position from which a compact tension sample was taken could influence the fatigue crack growth rate. In this study the funnel location during pouring (at the top center edge) was considered as a gate region, in analogy with injection molding, and thus the upper center of the plaque was assumed to be a high orientation region, as shown in Figure 2(a). To specifically determine the influence of orientation, samples were cut from the high orientation region either parallel or perpendicular to the presumed major flow (pour) direction. All other samples were cut from what were presumed to be lower orientation regions as shown in Figure 2(c). Also, to avoid edge effects, no samples were cut closer than 19 mm from the outer sides of the plaque. As an arbitrary choice, the crack was oriented parallel to the pour direction for all samples cut from the lower orientation regions.

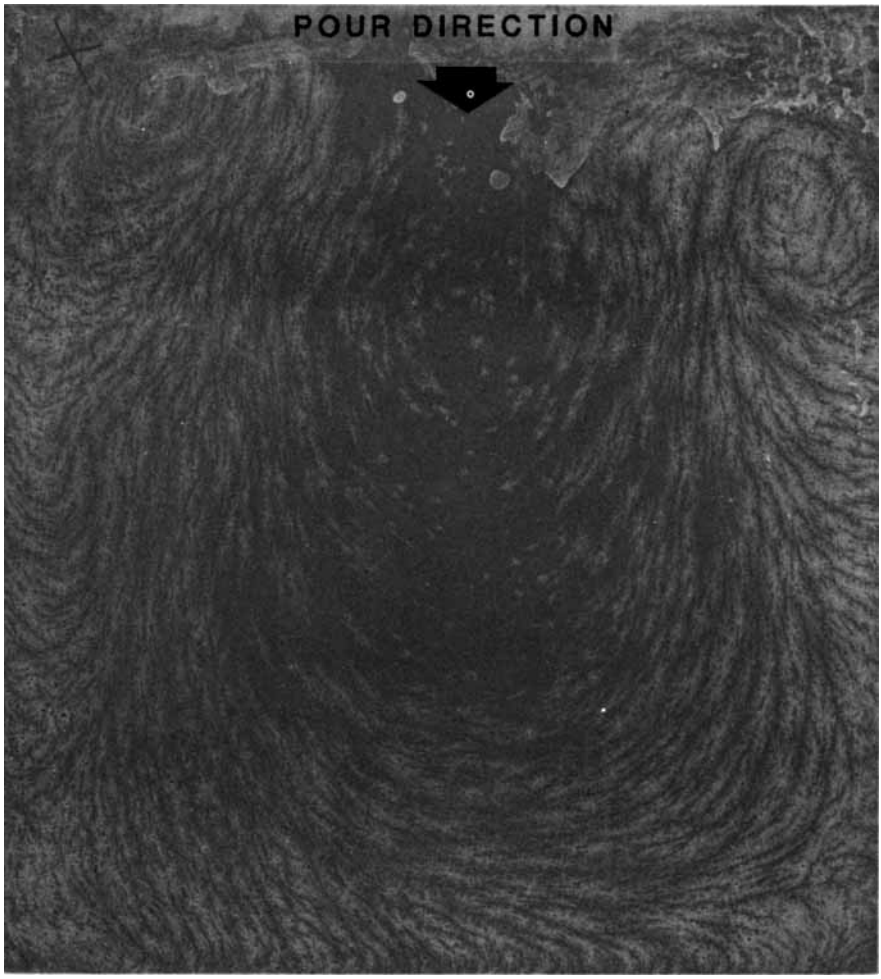


Fig. 1. Flow pattern shown by surface porosity in a hand-poured RIM nylon plaque.

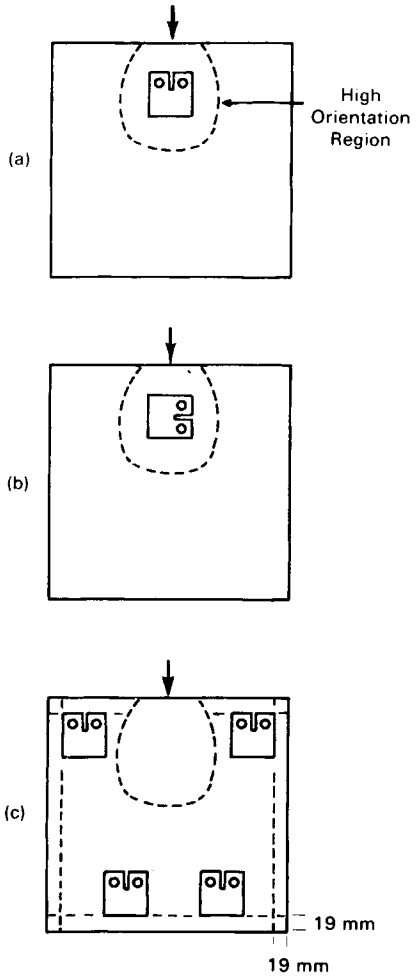


Fig. 2. Diagrams showing positions from which compact tension specimens were cut from RIM nylon plaques: (a) parallel to major flow direction (arrows); (b) perpendicular to major flow direction; (c) all others.

## Fatigue Crack Propagation

Samples for fatigue testing were machined into the form of compact tension specimens in accordance with ASTM E-647.[7] Samples were cut 61 × 63.5 mm and contained an initial saw cut of 22.9 mm. Fatigue cracks were initiated at a razor cut in the saw cut notch using the same oscillating loads using during the subsequent crack propagation measurements. Fatigue cycling was carried out under load control using an MTS closed loop servohydraulic testing machine. A sinusoidal wave form at a frequency of 5 Hz was employed and the $R$ value (minimum load to maximum load ratio) was set at 0.1.

Fatigue crack growth was monitored in real time using an MTI-65 video camera and recorder. Cracks were examined at magnifications ranging from 4 × to 60 × . Distances between features on the video tape were measured with a cursor system with the assigned voltages for each $x$, $y$ coordinate

position being converted to units of length by means of a calibrated tape on the face of the specimen. The video system also had a densitometer accessory with which the intensity of the video screen image could be accurately analyzed. The crack area was illuminated with a fiber optics light source, and relative intensities of the transmitted light were determined. This permitted accurate and reproducible location of the crack tip and also allowed measurement of the size of the deformation zones in the vicinity of the crack. In addition to the video camera, an infrared sensing thermography camera was employed to monitor sample temperature to insure that hysteretic heating at the crack tip was not occurring at the frequency employed.

## Data Analysis

From the measured crack length $a$ and the number of cycles, $N$, the incremental crack growth rate was calculated using a modified secant method as

$$\frac{da}{dN}(a_i) = \frac{a_{i+1} - a_{i-1}}{N_{i+1} - N_{i-1}}$$

This procedure worked well for the unfilled samples. However, in the case of the glass-filled materials the crack front grew in an irregular manner. In this case, crack growth rates were calculated graphically from a plot of $a$ vs. $N$ for each sample. Crack growth rates for the unfilled nylon 6 were shown to be equivalent using both techniques.

Fatigue crack propagation rates are normally expressed in terms of the associated stress intensity factor range $\Delta K$ and follow the Paris equation, which is[8]

$$\frac{da}{dN} = A(\Delta K)^m$$

where $A$ and $m$ are constants characterizing the material. The stress intensity factor at the crack tip is calculated from expressions based upon linear elastic fracture mechanics which are often used to describe fracture and fatigue behavior of nonlinear and heterogeneous materials.[9,10] In general the stress intensity factor is given by

$$K = \sigma\sqrt{\pi a}\, Y(a)$$

where $\sigma$ is the applied stress and $Y(a)$ is dependent on the specimen geometry.[10,11] The specific equation for $\Delta K$ for compact tension samples is

$$\Delta K = \frac{\Delta P}{B\sqrt{W}} \frac{(2+\alpha)}{(1-\alpha)^{3/2}}(0.886 + 4.64\alpha - 13.32\alpha^2 + 14.72\alpha^3 - 5.6\alpha^4)$$

where $\Delta P$ = maximum load − minimum load and $\alpha = a/W$ with $W$ being the sample width.

## RESULTS

### Tensile Properties

The results of the Instron testing are given in Table III. The tensile strength decreases for all glass filled samples, regardless of filler size. For nylon containing 33% of the silane treated 1/32 in. milled glass, the tensile strength is improved compared to untreated glass; however, it is still slightly less than that of the unfilled nylon 6. Tensile modulus increases with the addition of the glass fibers in all cases. For comparison, 33% glass fiber reinforcement of injection-molded nylon 6 (Capron 8233 from Allied Chemical) provides increased tensile strength (162 MPa) in addition to improved stiffness (9.3 GPa flexural modulus). Thus the tensile data alone suggest that the milled glass fibers are significantly less effective than conventional chopped glass fiber reinforcements.

### Fatigue Crack Propagation

**Unfilled Nylon.** Figure 3 shows the crack propagation data for unfilled RIM nylon 6. On a semilogarithmic plot the $da/dN$ vs. $\Delta K$ data is linear, indicating accordance with the Paris equation. The exponent $m$ is approximately 6. Results are shown for both the graphical method and the secant data reduction technique confirming their equivalence. Data from replicate samples also fell on the line shown in Figure 3. The comparison of results with previous literature on injection-molded nylon indicates that the crack propagation rates are generally faster in the RIM material. It is possible that the higher level of residual monomer and oligomers in the RIM sample contributes toward this reduced resistance to crack propagation, but the exact cause is unknown.

**Glass-Filled Nylon.** When untreated milled glass fibers were added to the RIM nylon 6, the phenomenology of the fatigue fracture process changed significantly. The crack not only grew in an irregular manner but also was surrounded by a very large damage zone. In spite of the different crack appearance for unfilled and glass-filled nylon 6 samples, the rate of crack propagation was very similar. Figure 4 shows data for RIM nylon 6 containing untreated 1/32 in. milled glass at two levels, 15 and 33% by weight. It is difficult to distinguish any clear effect of the glass fibers on crack growth rate when comparing these results to the unfilled sample (dashed line). A slight

TABLE III
Tensile Properties of RIM Nylon 6

| Milled glass | | Tensile strength | Tensile modulus |
|---|---|---|---|
| Amount (%) | Size (in.) | (MPa) | (GPa) |
| 0 | 0 | 85 | 2.4 |
| 15 | 1/32 | 74 | 3.8 |
| 33 | 1/32 | 49 | 3.6 |
| 33 | 1/16 | 54 | 3.8 |
| 33 | 1/32 (treated) | 76 | 4.9 |

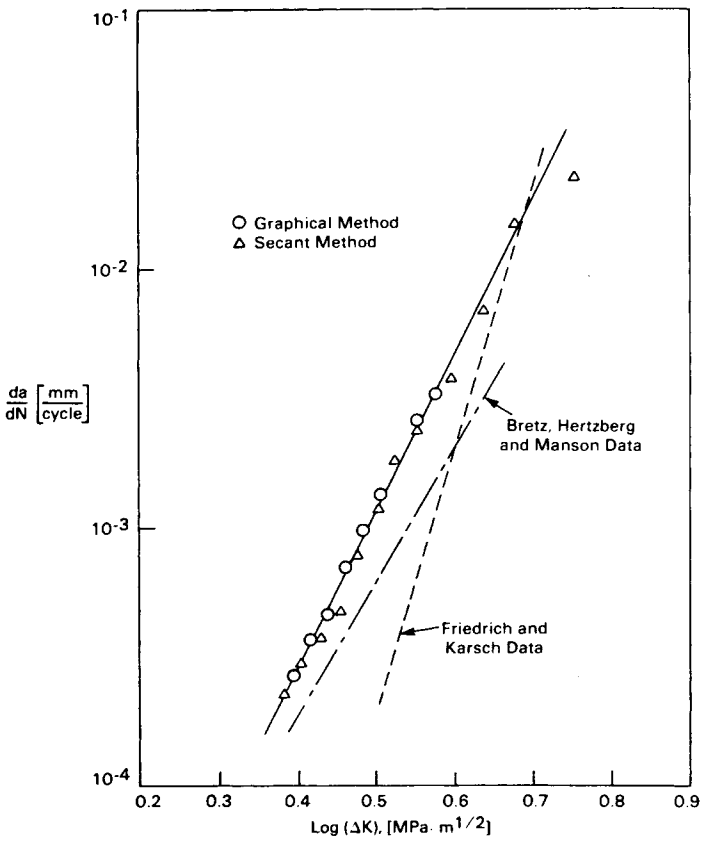


Fig. 3. Fatigue crack propagation rates for unfilled RIM nylon 6 vs. stress intensity factor range. Literature data are shown for comparison. (○) Graphical method; (△) secant method.

improvement is suggested at lower $\Delta K$ values; however, no conclusion can be drawn in view of the scatter in the data.

Samples cut from the high orientation region of the plaque did show a consistent trend with the lower crack growth rates corresponding to the perpendicular fiber orientation. This is shown in Figure 5. However, even in this case, there is little improvement suggested by incorporating the glass fibers.

A more definite improvement was observed by use of longer glass fibers. This is shown in Figure 6 where data for nylon 6 containing untreated 1/16 in. fibers can be compared with the unfilled sample (dashed line). In this case the presence of the fibers clearly improved the resistance to fatigue crack propagation. For example at a given $\Delta K$, cracks propagated about three times faster in unfilled nylon 6 than in the 33% glass-filled sample. Samples containing even longer glass fibers, 1/4 in., could not be prepared at the 33% filler level due to the high viscosity of the mixture. For comparison purposes data are also shown in Figure 6 for an injection molding grade nylon 6 which contains 33% chopped glass fibers. A much greater reduction in crack growth rate is observed with this material which not only has longer fibers but also

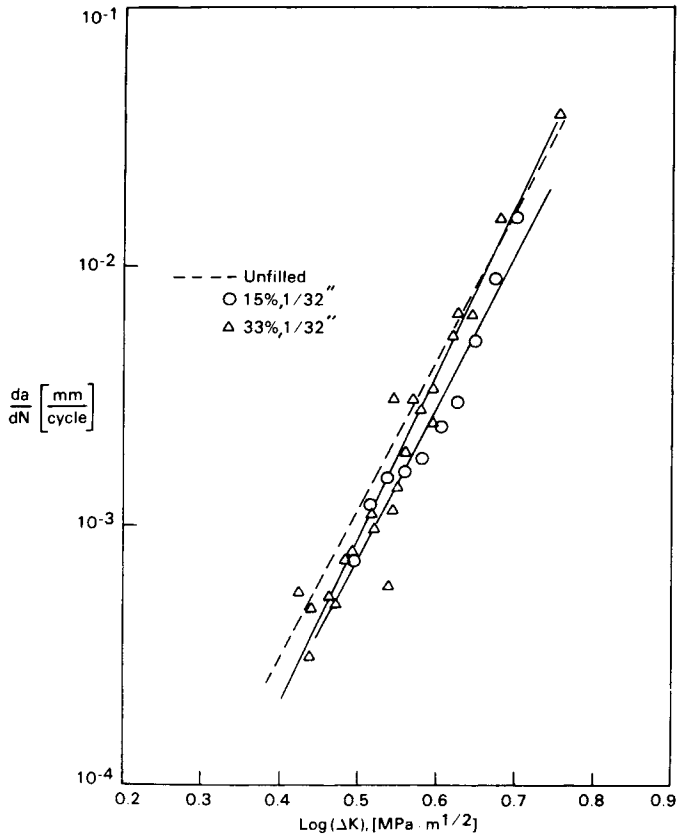


Fig. 4. Fatigue crack propagation rates for RIM nylon 6 containing 1/32 in. milled glass fibers: (- - -) unfilled; (○) 15%; (△) 33%.

was oriented during injection molding to provide alignment of the fibers in a direction perpendicular to the crack growth direction.

Since there were anticipated processing advantages to using the shorter milled fibers, attempts were made to improve fatigue resistance by the use of surface treatments. In fact, the glass fibers employed in the orientation study had been treated with a silane coupling agent to improve the adhesion between the fiber and the matrix. As noted previously, the silane treatment did improve the tensile strength of the milled glass filled RIM nylon. However, by comparing Figures 4 and 5 it can be seen that there is not a large effect of the coupling agent on the fatigue behavior. The surface treatment did have a dramatic effect on the appearance of the fatigue crack. Though the crack propagated along an irregular path, a damage zone was not readily apparent. This suggests that the damage is very directly related to the nylon–glass interface and is perhaps caused by void formation or microcracking which occurred in the absence of good adhesion. It also demonstrates an inverse relationship between damage zone size and yield stress since the yield stress was significantly higher for the sample with treated glass.

In spite of the evidence that the silane treatment improved the interfacial adhesion, there was unfortunately no corresponding retardation in fatigue

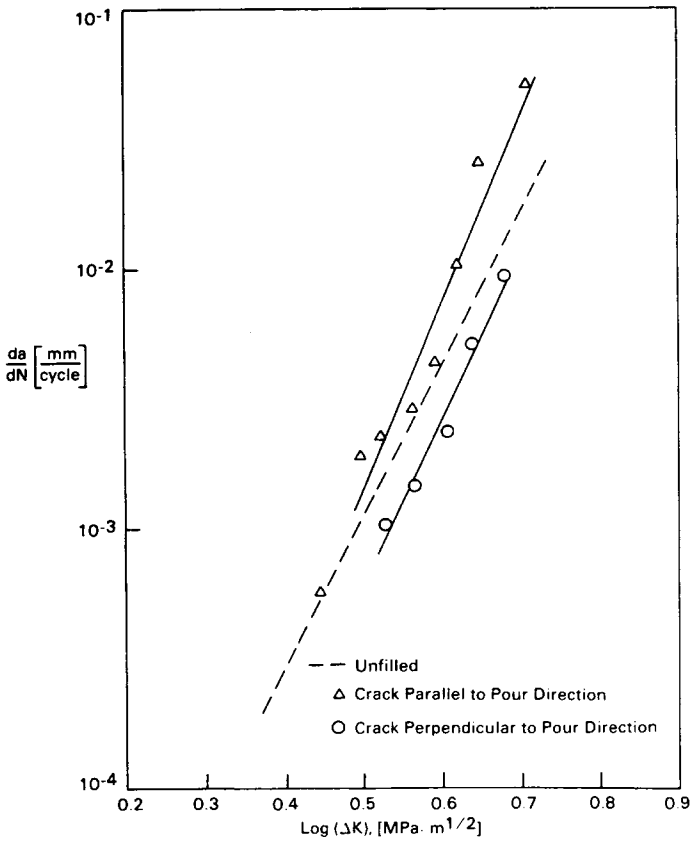


Fig. 5. Fatigue crack propagation rates for silane-treated 1/32 in. glass-fiber-reinforced RIM nylon 6 showing the effect of orientation: (---) unfilled; (△) crack parallel to pour direction; (○) crack perpendicular to pour direction.

crack growth rate. Thus the available results indicate that the first step toward improving fatigue resistance is to employ longer milled glass fibers.

## Crack Tip Appearance

**Unfilled RIM Nylon 6.** Photographs of the growing fatigue crack taken from the video recording are shown in Figure 7. For the unfilled nylon 6 the crack propagated perpendicular to the applied oscillating load in a relatively stable manner up until the transition to fast fracture. From a review of various crack open and crack closed video images, it was apparent that the overall crack length was in reality composed of a true crack plus a darkened zone ahead of the crack tip [Fig. 7(c)]. Although it is tempting to associate the darkened zone with a deformation zone, the fractography results suggest that the zone is due to the thumbnail shape of the crack tip. This is shown in Figure 8(a), where the thumbnail shape of the crack front is evident at the transition to fast fracture. The fatigue fracture surface of the reaction-molded nylon 6, as seen in Figure 8(b), exhibits a characteristic patchy morphology similar to that reported by Bretz et al. in their study of injection-molded

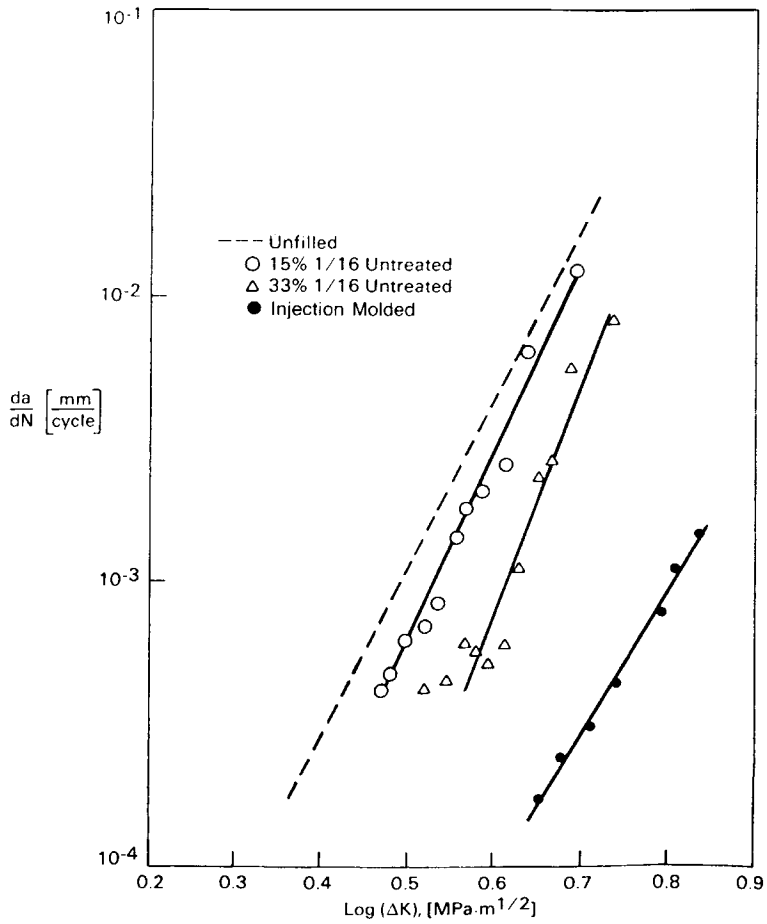


Fig. 6. Fatigue crack propagation rates for RIM nylon 6 containing 1/16 in. milled glass fibers. Data are also shown for injection-molded nylon 6 containing 33% chopped glass fibers: (- - -) unfilled; (○) 15% untreated; (△) 33% untreated; (●) injection-molded.

nylon 6.[2] This structure has been associated with a void coalescence type of mechanism. The patchy features are 50–150 $\mu$m in size and are not strongly affected by the increase in $\Delta K$. For comparison the spherulite size in similarly prepared reaction-molded plaques is of the order of 10–50 $\mu$m; thus the structure is not generally representative of the deformation of individual spherulites. It is also noteworthy that no surface striations, often associated with fatigue-type fracture surfaces,[5] or shear lips at the sample edges, were observed.

For comparison with the fatigue fracture surface a reaction-molded nylon 6 sample was also fractured under a constant tensile load in a creep rupture apparatus. A comparison of the fracture surfaces from fatigue and creep are shown in Fig. 9. Both modes of failure produce a similar patchy type of surface morphology. It is noted that there is more evidence of ductile tearing around the patchy regions of the fatigue fractured surface and also the fracture plane is more uneven for the constant load failure. Whether these

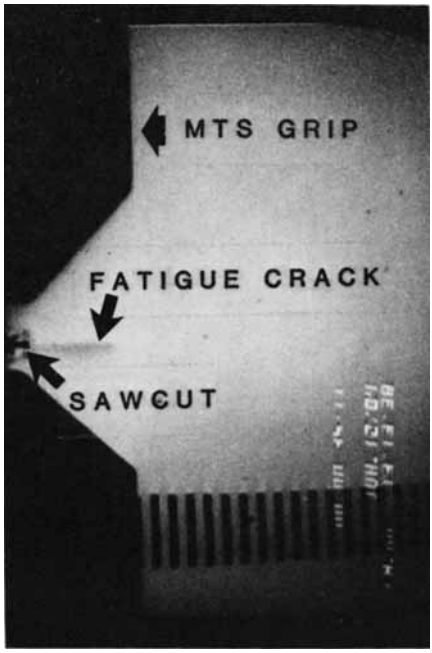


(a)

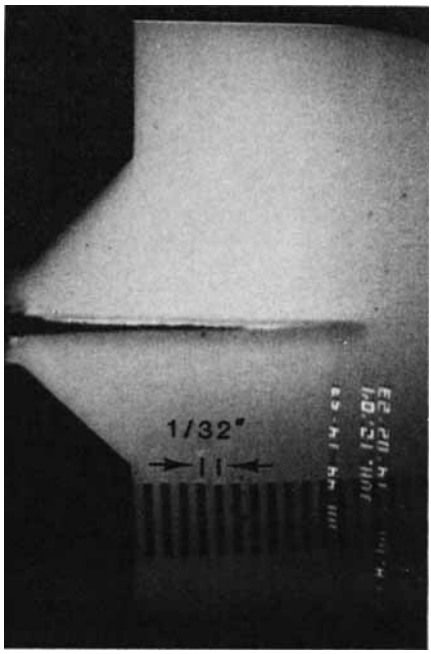


(b)

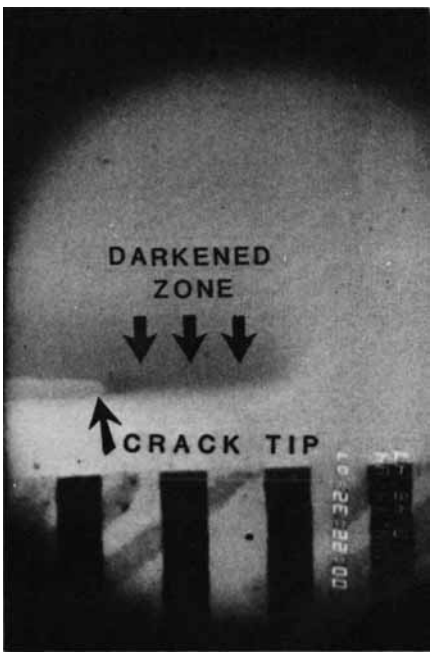


(c)

Fig. 7. Fatigue crack appearance in unfilled RIM nylon 6 showing: (a) initial stage of cracking; (b) crack open position during stable propagation stage; (c) high magnification view of crack tip.

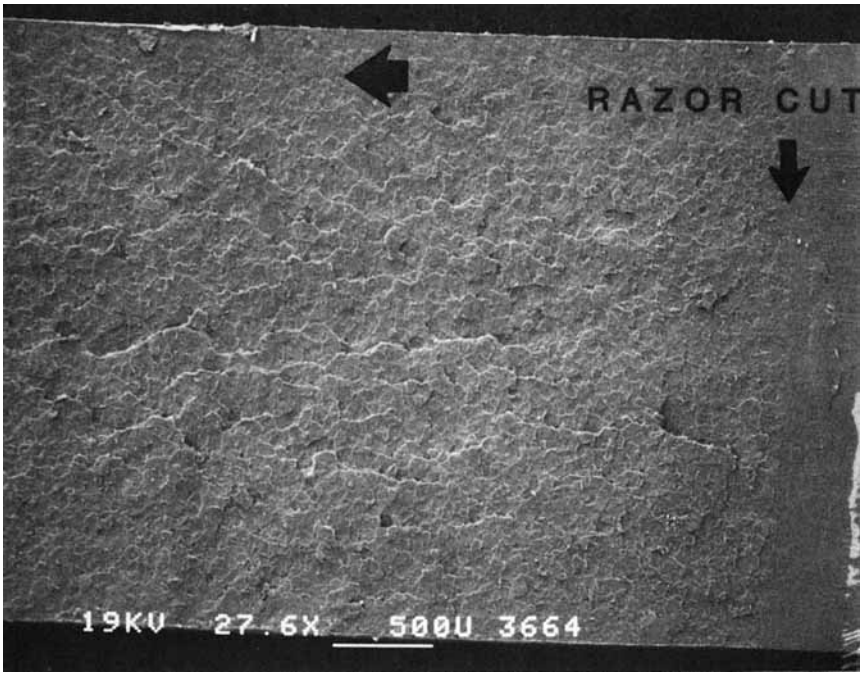


(a)

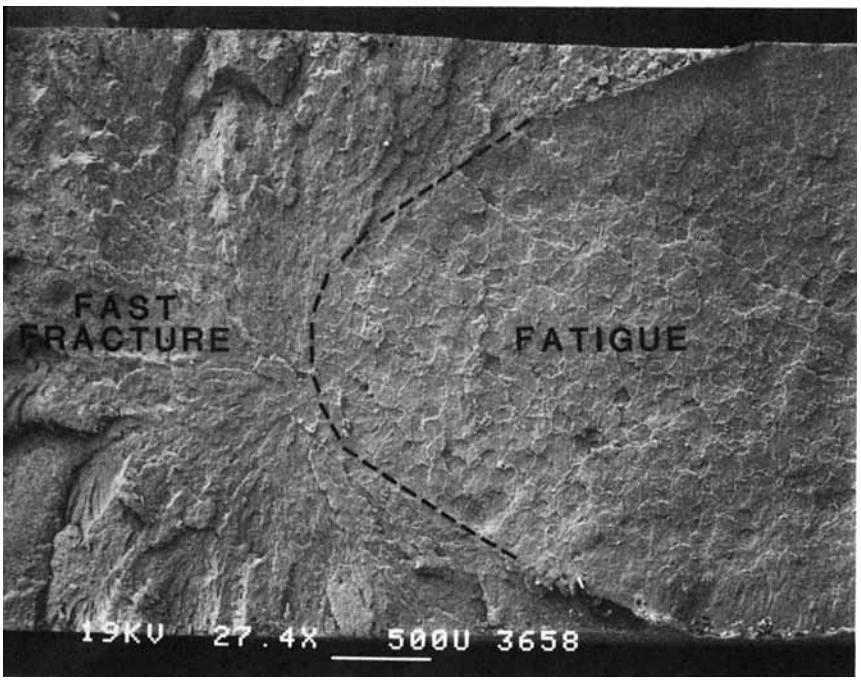


(b)

Fig. 8. Fracture surface of unfilled RIM nylon 6 showing: (a) initiation from razor cut; (b) transition to fast fracture (unstable crack propagation). Magnification: 27 ×. Large arrows indicate crack growth direction in this and subsequent figures.

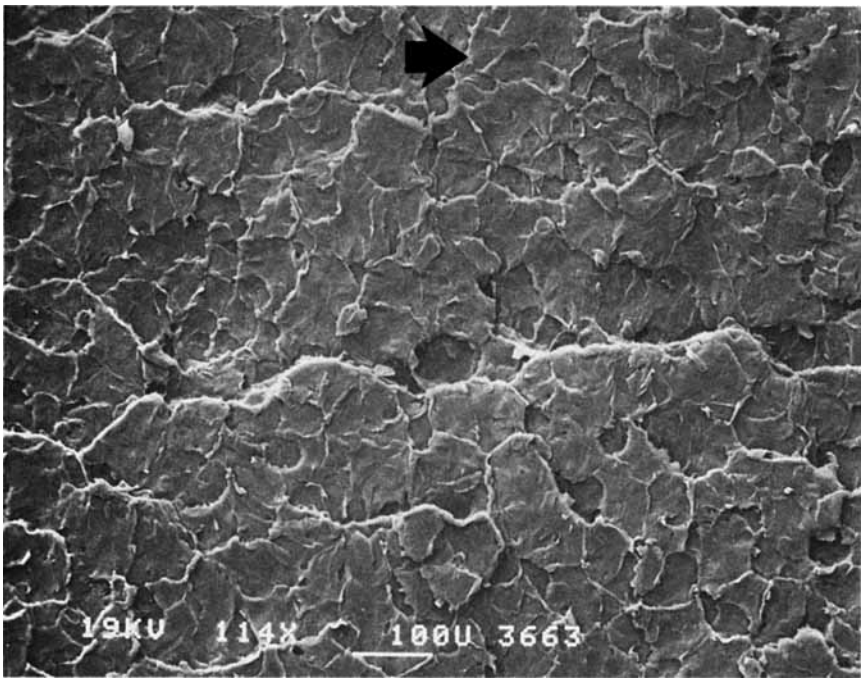


(a)

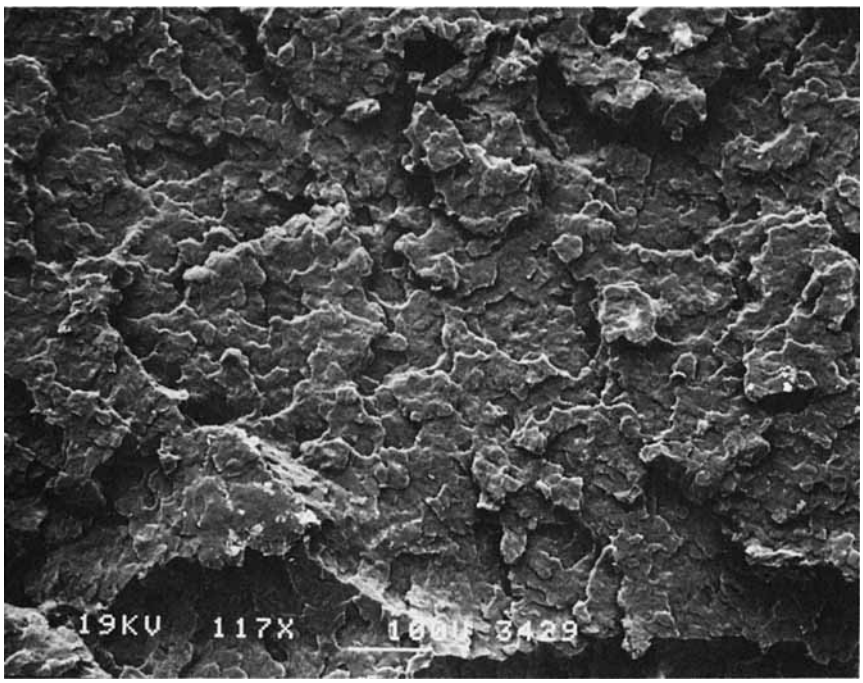


(b)

Fig. 9. Fracture surface of unfilled RIM nylon 6 subjected to: (a) fatigue loading, 114×; (b) constant load, 117×.

differences are due to the mode of loading (oscillating vs. constant) or to strain rate effects is not clear. Constant load fractures of additional RIM nylon samples which were partially moisturized, and of dry injection-molded samples, also exhibited patchy type structures with generally more evidence of ductility. Thus it is clear that this type of fracture surface is not unique to fatigue. It is somewhat surprising that the presumably incremental crack growth during fatigue loading did not produce unique striations or other features to more clearly differentiate stable fatigue cracking from the monotonic crack propagation produced by the creep rupture test. A possible explanation is that the fatigue crack growth does involve a creep mechanism rather than a true fatigue process. This is currently being further investigated.

**Glass-Filled RIM Nylon 6.** Figure 10 shows the propagation of a fatigue crack in RIM nylon 6 reinforced with 33% by weight of the untreated 1/32 in. milled glass fibers. Compared to the unfilled material, the crack propagated in a much more irregular manner, although the overall direction of crack growth is still perpendicular to the applied load. In addition, Figure 10 shows that there is significant damage in the matrix surrounding the crack with an intense zone of damage (darkening) at the crack tip. At higher magnifications the damage zone near the crack tip was seen to be composed of feathery-like microcracking, also illustrated in Figure 10. It was not possible to clearly focus the microcracking pattern, perhaps indicating that it was internal to the sample rather than on the surface. The microcracking is randomly oriented and occupies a symmetrically shaped area in the immediate vicinity (1 mm) of the crack tip. There was no evidence of a line-shaped zone of darkening as was observed in the unfilled sample. Thus the presence of the glass fibers dramatically modifies the macroscopic appearance of the deformation in advance of the propagating fatigue crack.

The nature of the damage events in the milled glass-filled RIM nylon 6 was investigated by examining the fracture surfaces as shown in Figure 11. Little or no adhesion between fiber and matrix is suggested in the initiation and propagation regions of the stable fatigue fracture surface. The propagation region is distinct in showing more plastic deformation of the nylon matrix (points labeled A). Even the holes from glass fiber pullout are deformed (points labeled B), and the holes are enlarged compared to the initiation region. In the fast fracture region the cleavage is more brittle with occasional indications of adhesion of matrix material to the glass fibers (points labeled C) and much less indication of voided regions (points labeled D) or wells around the fibers.

The fractography results are compatible with the idea that fiber–matrix debonding is responsible for the visually observed damage zone. Microtomed through-thickness views also revealed extensive void formation and microcracking around the glass fibers as shown in Figure 12. Unfortunately, the microtoming process could not define the specific area of the damage zone since some degree of microcracking occurred during sectioning of the samples. Side views of the fracture path were also examined for evidence of fiber–matrix debonding. Surprisingly no indication of failure or deformation around the glass fibers was seen [Fig. 12(b)], even at higher magnifications. Thus it is concluded that most of the damage sites causing the darkened zone are internal to the sample. A sample of particular interest was the RIM nylon 6

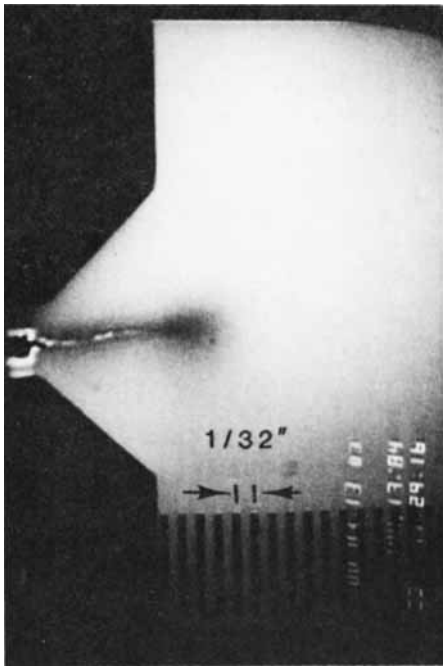


(a)

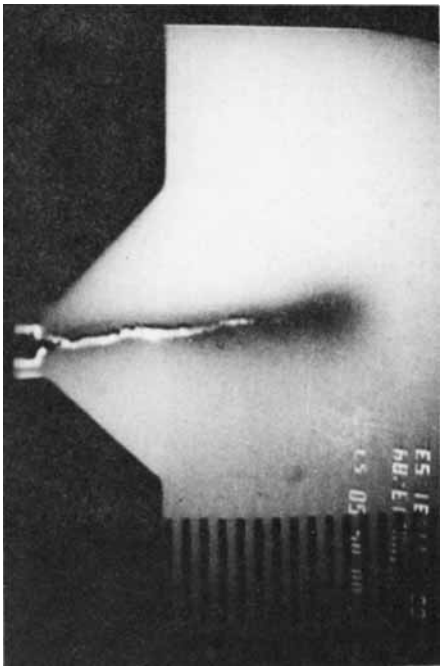

(b)

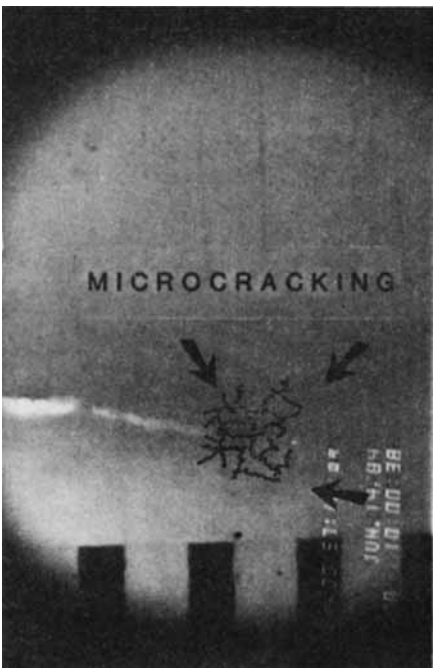


(c)

Fig. 10. Fatigue crack appearance in glass-filled RIM nylon 6 showing: (a) initial stage of cracking; (b) crack open position during stable propagation stage; (c) high magnification view of crack tip with microcracking pattern artificially enhanced.


(a)

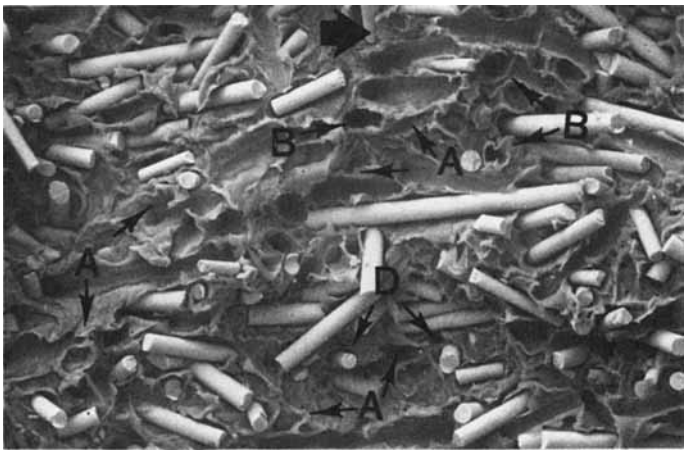


(b)

Fig. 11. Fatigue fracture surface for RIM nylon 6 containing untreated milled glass fibers showing: (a) initiation; (b) propagation; (c) fast fracture regions. Arrows demonstrate: (A) matrix drawing; (B) deformed holes after fiber pullout; (C) fiber–matrix bonding; (D) voided regions around fibers. Magnification: 220 ×.

containing milled glass fibers treated with a silane coupling agent. As mentioned earlier, this sample did not exhibit a large damage zone. Figure 13 shows the fractography results with views of the initiation, propagation, and fast fracture regions. The initiation region is quite similar to that observed in Figure 11 for the sample containing untreated fibers with the exception that a considerable amount of debris, presumed to be particles of broken glass fibers, is noted. A closer examination of the entire fracture surface indicated that the debris was confined to an area in the center of the sample adjacent to the razor blade cut precrack. Although at first thought to be an anomaly, debris was also observed in a review of other micrographs near the initiation site. However, it was not possible to clearly define the size of the debris region or amount of debris in repeated fatigue experiments. The debris seen on the


(c)

Fig. 11. (*Continued from the previous page.*)

fracture surface will require further study before it is clearly understood; however, it is presently believed that it is caused by extensive glass fiber fracture during the early stages of crack growth when the specific fracture path is determined, if not demanded, by the razor cut precrack.

Figure 13 also shows the stable fatigue crack propagation region of the fracture surface for the nylon 6 containing treated glass fibers. In spite of the silane treatment on the glass fibers, it is difficult to distinguish this fracture surface from the one shown in Figure 11 for nylon containing untreated fibers. Clear evidence of fiber–matrix debonding, fiber pullout, and deformation (enlargement) of the holes around the fibers can be seen. Extensive ductile tearing of the nylon matrix is also noted. The results suggest that debonding occurred prior to fiber pullout; otherwise smaller holes would be evident. In marked contrast to the propagation region, the fast fracture shows the brittle nature of the final cleavage. The micrograph shown in Figure 13(c) indicates that ductile tearing of the nylon matrix is no longer apparent nor is there evidence of debonding of fibers. In fact, excellent fiber–matrix adhesion seems to be the case. This differs from the results shown in Figure 11(c) for the untreated glass. These results confirm the uniqueness of the fracture surface for fatigue failure in the glass-filled RIM nylon materials and further demonstrate that the extensive fiber debonding is not due to poor initial fiber–matrix adhesion.

## Damage Zone Analysis

Although the milled glass fibers do not provide an effective means of improving the fatigue resistance of RIM nylon 6, the video method of observing crack propagation in such filled systems appears to offer promise in delineating the nature of the damage process at the crack tip. For example, it was possible to characterize the size of the diffuse damage zone that developed in the untreated glass-filled samples by using a densitometer to analyze the intensity of the image on the video screen. Figure 14 shows the

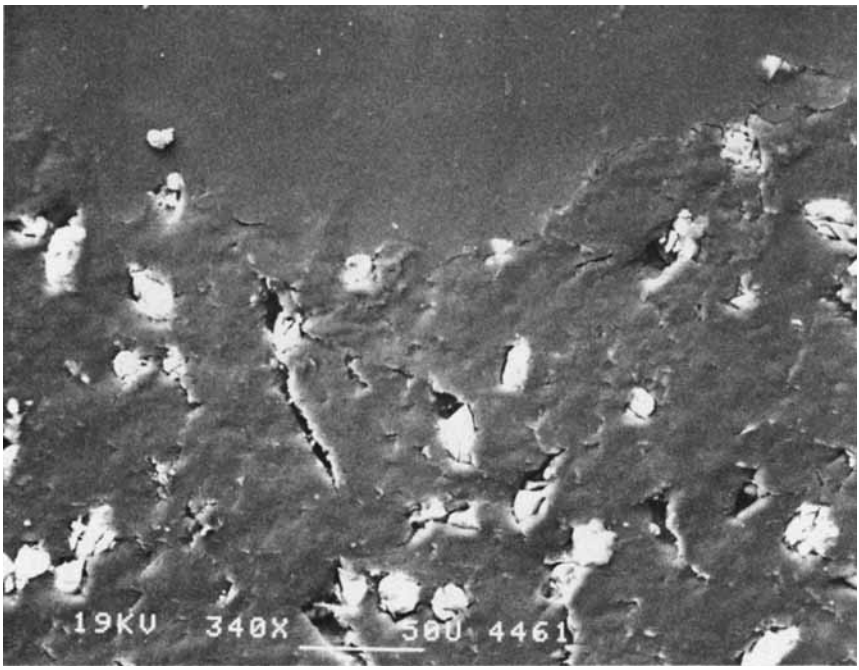


(a)

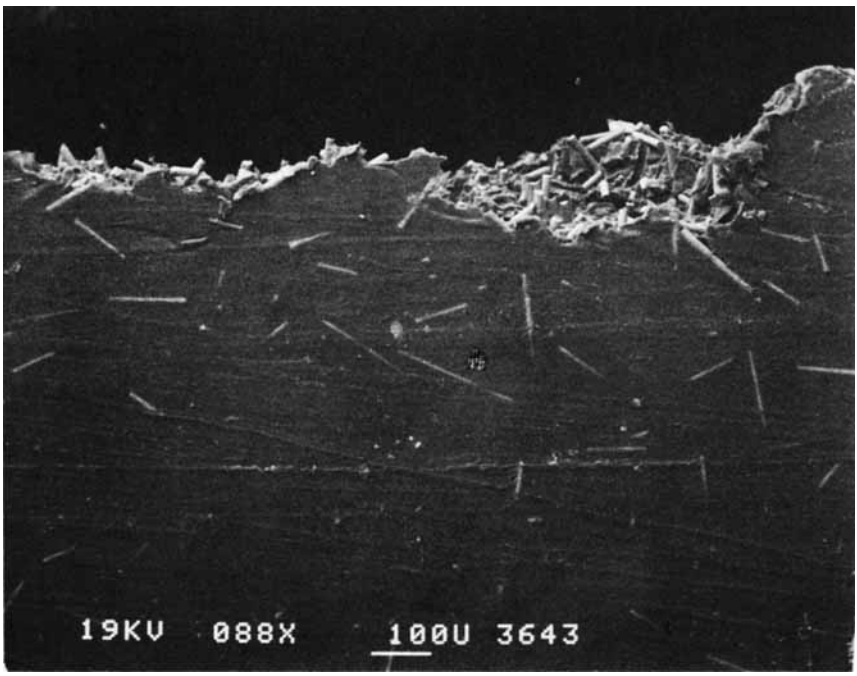


(b)

Fig. 12. Scanning electron micrographs of fatigue-fractured glass-filled RIM nylon 6: (a) transverse section showing microcracking beneath the surface; (b) side view showing no obvious fiber debonding or microcracking. Magnifications: (a) 340 ×; (b) 88 ×.

(a)

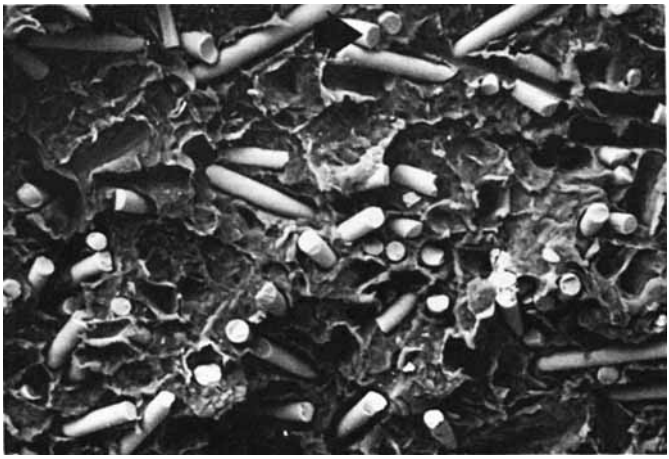

(b)

Fig. 13. Fatigue fracture surface for RIM nylon 6 containing silane-treated glass fibers showing: (a) initiation; (b) propagation; (c) fast fracture regions. Magnification: 275 ×.

densitometer trace and associated intensity profile superposed on the video image. With the densitometer trace located along the direction of cracking [Fig. 14(a)], the crack tip position is apparent from the peak in intensity. Also, the extent of the damage zone (darkening) in advance of the crack tip is easily seen. In Figure 14(b) the densitometer trace is located on the right edge of the damage zone which was easily defined by positioning the trace where no change in the slope of the intensity profile occurred. A similar measurement on the left edge resulted in a rough outline of the outer limits of the damage zone as shown in Figure 14(c). It is immediately apparent that the outer limits of the damage zone defined by the densitometer are much larger than that observed visually. Moreover, even the damage zone dimensions defined by the densitometer may be arbitrary since more intense illumination or more sensitive image analysis might extend the limits further. Still, for the conditions

(c)

Fig. 13. (*Continued from the previous page.*)

employed, an extremely accurate estimate of the damage zone size is possible with the densitometer system.

Figure 15 shows a contour map of the damage zone at an intermediate stage of crack growth. Both the onset of darkening and the points at which the intensity is half that in the undamaged region are shown. The fact that the region of 50% darkening increased significantly in front of the crack tip (where the stress intensity is highest) suggests that the damage sites were enlarged or the number of damage sites was increased by the higher stress levels.

The elastic nature of the damage zone size as well as the effect of stress level is shown even more directly by examining the crack tip in the crack open (maximum stress) and crack closed (minimum stress) positions. This is shown photographically in Figure 16 and in the contour maps of Figure 17. Both figures demonstrate the extent to which the size of the damage zone increases in the more highly stressed crack open position. This effect was clearly evident in viewing the video tape since the darkened region pulsated during cyclic loading. The pulsating was not as evident along the edges of the crack as it was at the tip. From these results it is clear that the damage zone exhibits both a dynamic and a static or nonrecoverable component.

It was of interest to compare the size of the damage zone in glass-filled RIM nylon with the predictions of plastic zone size suggested by linear elastic fracture mechanics. The latter predicts a 3-dimensional cylindrically shaped plastic zone which in cross section would be circular, as is (approximately) the observed damage zone. For conditions of plane stress the radius of the plastic zone at the crack tip should be[5]

$$r_y = \frac{1}{2\pi}\left(\frac{K_{\max}}{\sigma_y}\right)^2$$

where $K_{\max}$ is the maximum stress intensity and $\sigma_y$ the yield stress. From the

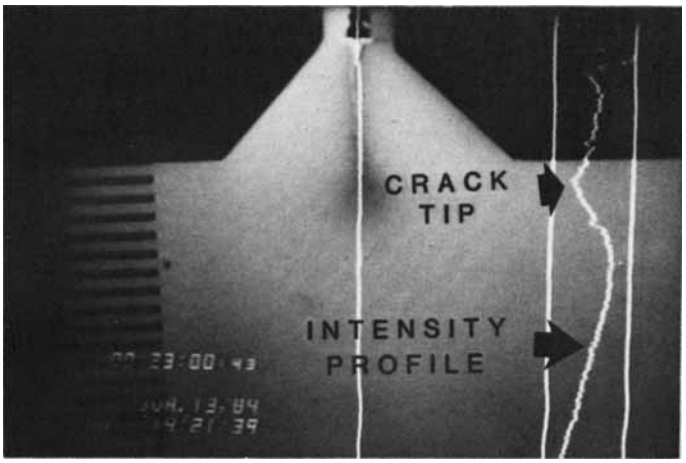


(a)

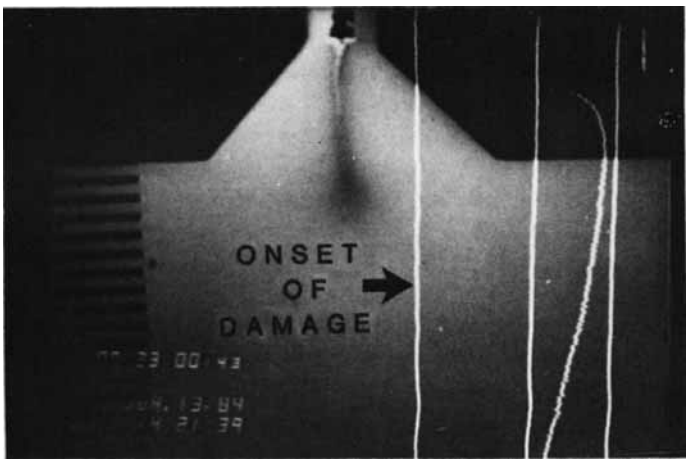


(b)

Fig. 14. Densitometer image analysis of fatigue crack in glass-filled RIM nylon 6 showing: (a) positioning of trace along crack with the corresponding intensity profile; (b) trace at outer boundary of damage zone; (c) 2-dimensional outline of outer limits of damage zone. Magnification: 4 ×.

densitometer analysis, $r_y$ was approximated to give an average radius near the crack tip as $(w + c)/3$, where $w$ and $c$ are shown in Figure 17(b). A plot of $r_y$ vs. $(K_{max})^2$ should be linear according to the above equation and such behavior has been observed in rubber toughened blends.[12] Figure 18 shows the dependence of $r_y$ on $(K_{max})^2$ for the 33% glass-filled nylon. Initially a linear dependence is suggested with the straight line passing through zero as it should, i.e., if $K_{max}$ is zero, there should be no plastic zone. However, at the higher $K_{max}$ levels, corresponding to longer crack lengths and increasing crack speeds, a point is reached where the radius of the damage zone remained relatively constant. From the slope of the initial straight line portion it is possible to calculate the apparent yield stress in the damage zone from the $r_y$

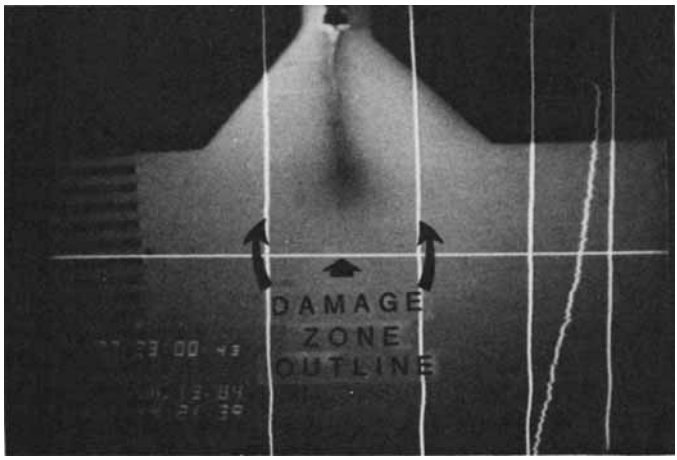


(c)

Fig. 14. (*Continued from the previous page.*)

relationship. A value of 27 MPa was obtained which is much less than the value of 49 MPa determined from tensile measurements.

This lack of agreement together with the observed nonlinearity in Figure 18 may be taken as evidence that linear elastic fracture mechanics does not apply to the heterogeneous glass-filled material. Clearly the size of the damage zone is very large in relation to the sample thickness, which violates an assumption of the plastic zone model. However, it may also be possible that the lower stress (27 MPa) relates to that required to initiate fiber–matrix debonding, whereas the higher value of 49 MPa was the stress required for complete

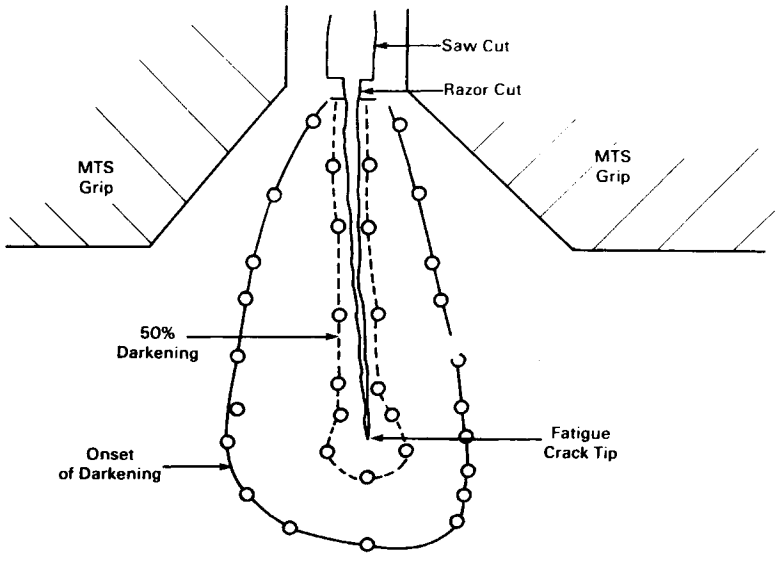


Fig. 15. Profile of the damage zone surrounding a fatigue crack in milled glass-filled RIM nylon 6. Both the onset of darkening and the zone of 50% darkening are shown.

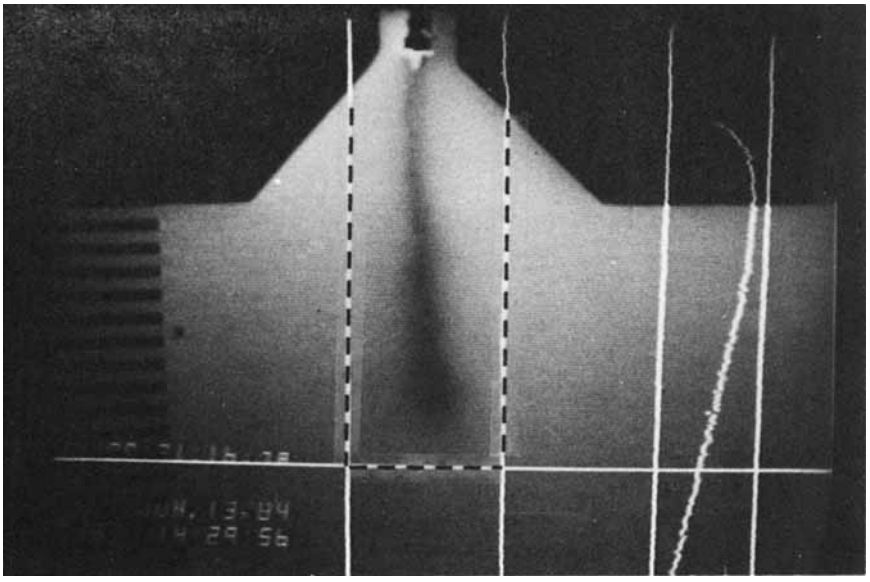

(a)

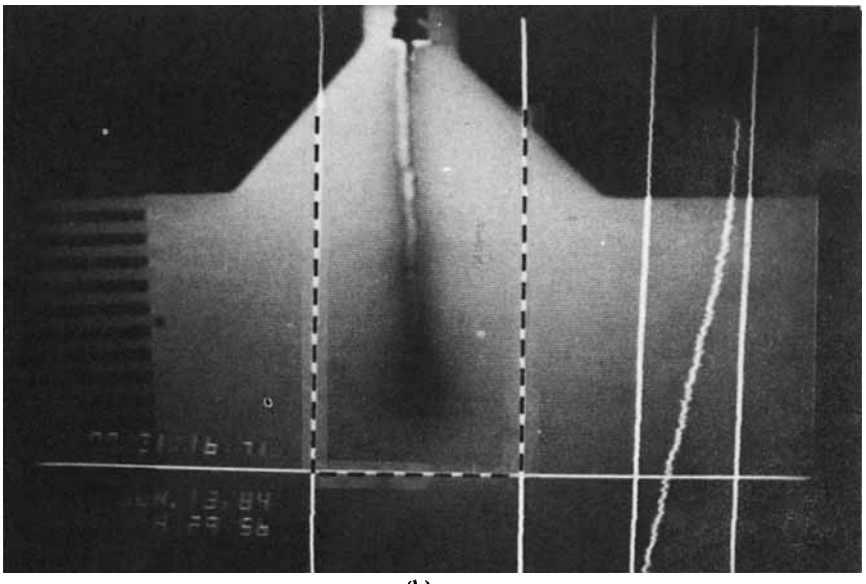

(b)

Fig. 16. Photographs showing the outline of the damage zone with: (a) crack closed; (b) crack open illustrating the effect of stress intensity on the relative damage zone size.

rupture of the material. Thus further analysis may demonstrate the applicability of the linear elastic model, at least for the lower $K_{max}$ values.

An additional analysis of the damage zone volume was made in order to assess its relationship to the fatigue crack growth conditions. From the contour map studies, it was apparent that the cross-sectional area of the total

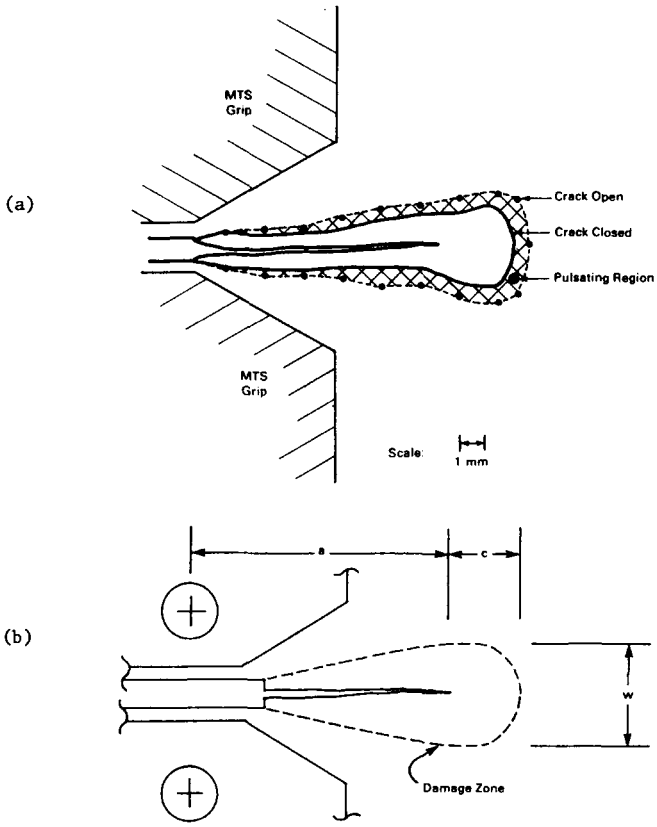


Fig. 17. (a) Damage zone profiles for both the crack open and crack closed positions showing the pulsating region; (b) schematic view of the damage zone showing the definition of the width $w$ and length $c$ of damage surrounding a fatigue crack of total length $a$.

damage could be approximated by assuming a linearly increasing damage zone width along the crack, plus a semicircular area of damage in front of the crack tip. By multiplying each of these contributions by the sample thickness, the volume of the damage zone can be calculated as

$$V_{dz} = (a_t - a_0)w_a t_s + \tfrac{1}{2}\pi\left(\frac{w + c}{3}\right)^2 t_s$$

where $V_{dz}$ = volume of damage zone, $a_t$ = crack length at time $t$, $a_0$ = initial crack length, $w_a$ = average width of damage zone, $t_s$ = thickness of the sample, $w$ = damage width at $a$ (see Fig. 17), and $c$ = damage length beyond $a$ (see Fig. 17).

The value of $w_a$ was calculated using the approximation

$$w_a = \frac{\sum_{i=1}^{j}(w_{i-1} + w_i)/2(a_i - a_{i-1})}{a_j}$$

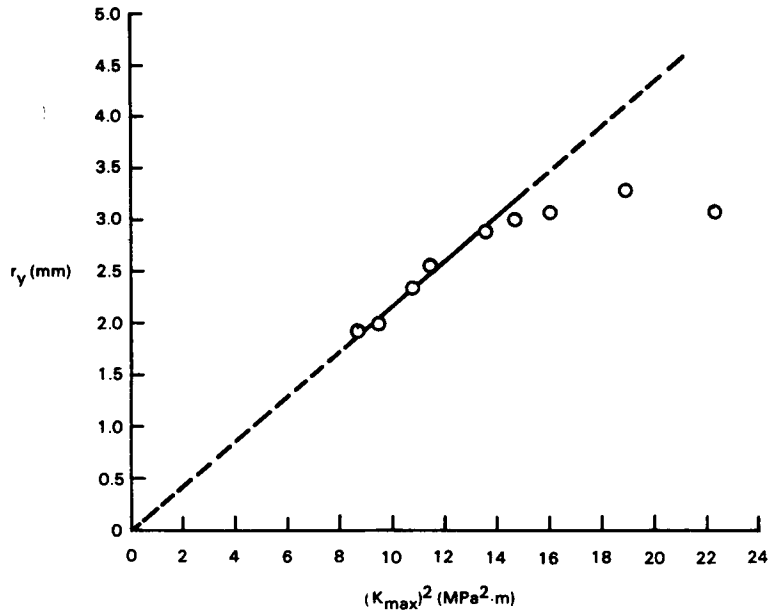


Fig. 18. Comparison of the experimentally measured damage zone radius of glass-filled RIM nylon 6 (data points) with the theoretically predicted plastic zone radius $r_y$ vs. the square of the maximum stress intensity factor.

This approximation simply replaces the trapezoidal area increment with an equivalent rectangular area.

The rate of growth of the damage zone volume with number of cycles, $N$, is then given by

$$\frac{dN_{dz}}{dN} = t_s w_a \frac{da}{dN} + t_s(a - a_0)\frac{dw_a}{dN} + t_s \pi r \frac{dr}{dN}$$

where $r$ is equated with $(w + c)/3$.

From the values of $w$, $c$, and $a$ measured from the videotape at selected values of $N$, and the values of $da/dN$, $dw_a/dN$, and $dr/dN$ calculated using the secant method, the growth of the damage zone volume was determined. Results are shown in Figure 19 where the change in damage zone volume per fatigue cycle is plotted against the stress intensity factor range. The log–log plot results in a linear relationship over the entire $\Delta K$ range. This indicates that the rate of change in damage zone volume per fatigue cycle, like the crack growth rate data (Fig. 4), follows a mathematical form given by the Paris equation, i.e.,

$$\frac{dV_{dz}}{dN} = B(\Delta K)^n$$

A value of $n$ of about 5 is obtained from the slope of the line in Figure 19 whereas the exponent was near 6 from the crack growth data. This similarity demonstrates an important connection between the growth of the actual

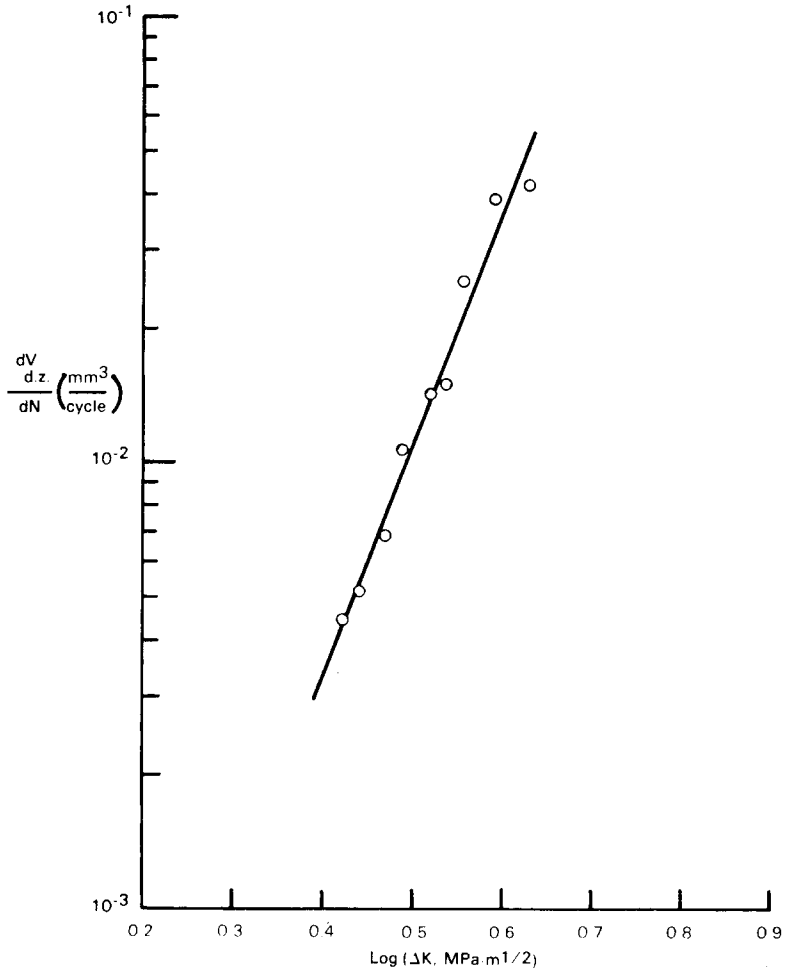


Fig. 19. Rate of change of damage zone volume $V_{d,z}$ per fatigue cycle $N$ as a function of the stress intensity factor range, $\Delta K$, for glass-filled RIM nylon 6.

fatigue crack and the damage surrounding that crack. Comparing Figures 18 and 19, it is also apparent that unlike the damage zone radius the damage zone volume does not level off at higher $K_{max}$ values and thus the volume may be a more meaningful parameter for characterizing the crack growth process.

## DISCUSSION

The fatigue crack propagation measurements demonstrate that the Paris law is followed for RIM nylon 6 just as it is followed for conventional injection molded nylon. In spite of the higher molecular weight of the RIM nylon 6 and a higher crystallinity,[13] the crack growth rate is faster than reported data for injection-molded nylon 6. This difference is tentatively attributed to the plasticizing effect of the residual monomer in the reaction-molded material. Of even greater significance is the comparison of the fatigue

behavior of glass-filled RIM nylon and glass-reinforced injection-molded nylon. The latter shows a manifold increase in fatigue resistance whereas the milled glass fibers in RIM nylon offer either no improvement or only marginal improvement. The lack of a significant effect for the milled glasses is attributed to the preponderance of short fiber lengths in this type of glass. This was confirmed by direct observation of the glass fibers after burning off the nylon matrix; however, quantitative fiber length distributions were not measured. The available results show that the use of longer milled glass fibers and orienting the fibers perpendicular to the crack growth direction are both methods to retard the fatigue crack growth rates. The role of glass coupling agents is not clear from the results of this study, though literature reports indicate this is also a method to retard crack propagation rates.[3,5]

It is clear that the fracture surface produced by stable fatigue crack propagation is distinctly different from that produced during fast fracture. This was observed for both the unfilled and the glass-filled RIM nylon 6. In general, the fracture surface morphologies for the reaction-molded nylon are similar to those previously reported for injection-molded materials. The absence of characteristic fatigue striations can be attributed to the fact that all of the samples were examined in the dry-as-molded condition.[3] Although such a dry state is usually associated with a brittle fracture mode, it is clear from the fractography that the fatigue fracture process involves localized ductile drawing of the nylon 6 matrix. This feature of the fatigue fracture was common to all of the samples examined, whether filled or unfilled, and whether the glass was treated or untreated.

The observation and analysis of damage zones at the fatigue crack tip using the video system offers promise as a unique method to characterize these materials. Extensive damage zones were noted for all nylon 6 samples containing untreated glass fibers, including the material filled with 1/16 in. fibers, which exhibited the best fatigue resistance. Though a large damage zone was not apparent in filled samples with silane-treated glass, the use of higher magnifications and alternative illumination may permit quantitative measurement of the deformation zones in this type of sample as well. This expectation is supported by the similar fracture surface appearance for untreated and treated glass-filled samples. This similarity, in marked contrast to the dissimilar damage zones, suggests that the materials undergo similar microdeformation prior to fracture and perhaps only the extent of localization of damage away from the crack tip may distinguish the two samples.

Of particular interest is the finding that the damage zone has a pulsating or active region as well as a nonrecoverable permanently damaged region. Obviously this aspect of characterizing the size of the damage zones underscores the usefulness of the video technique since measurements of unstressed samples would give erroneous results. Recent theories have discussed the value of using quantitative measures of damage to arrive at material constants which relate to fracture energies in composites as well as unfilled polymers.[14-17] It would appear that some measure of the damage profile in the thickness direction is necessary to correctly estimate damage zone volumes, especially in view of the lack of observable damage (microcracking) on the outer surface of the fatigue cracked sample. This approach is currently being further investigated for treated glasses of various fiber lengths.

## References

1. P. E. Bretz, R. W. Hertzberg, and J. A. Manson, *J. Mater. Sci.*, **16**, 2061 (1981).
2. P. E. Bretz, R. W. Hertzberg, and J. A. Manson, *J. Mater. Sci.*, **16**, 2070 (1981).
3. R. W. Lang, J. A. Manson, and R. W. Hertzberg, *Polym. Eng. Sci.*, **22**(15), 982 (1982).
4. M. T. Hahn, R. W. Hertzberg, and J. A. Manson, *J. Mater. Sci.*, **21**, 31 (1986).
5. R. W. Hertzberg and J. A. Manson, *Fatigue of Engineering Plastics*, Academic, New York, 1980, p. 130.
6. J. D. Gabbert, A. Y. Garner, and R. M. Hedrick, *Polym. Compos.* **4**(3), 196 (July 1983).
7. American Society for Testing and Materials, *1983 Annual Book of ASTM Standards*, Am. Soc. Testing and Mater., Philadelphia, 1983, Sec. 3, Vol. 03.01, E647-83, p. 718.
8. P. C. Paris and K. Erdogan, *J. Basic Eng. Trans. ASME*, **D85**, 528 (1963).
9. J. A. Manson and R. W. Hertzberg, *Crit. Rev. Macromol. Sci.*, **1**, 433 (1973).
10. S. T. Rolfe and J. M. Barsom, *Fracture and Fatigue Control in Structures*, Prentice-Hall, Englewood Cliffs, NJ, 1977.
11. R. W. Hertzberg, *Deformation and Fracture Mechanics of Engineering Materials*, Wiley, New York, 1976.
12. T. A. Morelli and M. T. Takemori, *J. Mater. Sci.*, **18**, 1836 (1983).
13. M. G. Wyzgoski and G. E. Novak, *J. Mater. Sci.*, **22**, 2615 (1987).
14. A. Chudnovsky, A. Moet, R. J. Bankert, and M. T. Takemori, *J. Appl. Phys.*, **54**(10), 5562 (1983).
15. A. Moet and A. Chudnovsky, *J. Mater. Sci.*, **20**, 630 (1985).
16. K. Sehanobish, E. Baer, A. Chudnovsky, and A. Moet, *J. Mater. Sci.*, **20**, 1934 (1985).
17. N. Haddauoi, A. Chudnovsky, and A. Moet, *Polymer*, **27**, 1377 (1986).

Received May 25, 1988
Accepted June 18, 1988